The JWST/NIRCam coronagraph: mask design and fabrication

John E. Krist, Kunjithapatham Balasubramanian, Charles A. Beichman, Pierre M. Echternach, Joseph J. Green, et al.

John E. Krist, Kunjithapatham Balasubramanian, Charles A. Beichman, Pierre M. Echternach, Joseph J. Green, Kurt M. Liewer, Richard E. Muller, Eugene Serabyn, Stuart B. Shaklan, John T. Trauger, Daniel W. Wilson, Scott D. Horner, Yalan Mao, Stephen F. Somerstein, Gopal Vasudevan, Douglas M. Kelly, Marcia J. Rieke, "The JWST/NIRCam coronagraph: mask design and fabrication," Proc. SPIE 7440, Techniques and Instrumentation for Detection of Exoplanets IV, 74400W (19 August 2009); doi: 10.1117/12.826448

SPIE.

Event: SPIE Optical Engineering + Applications, 2009, San Diego, California, United States

The JWST/NIRCam coronagraph: mask design and fabrication

John E. Krist[a], Kunjithapatham Balasubramanian[a], Charles A. Beichman[a], Pierre M. Echternach[a], Joseph J. Green[a], Kurt M. Liewer[a], Richard E. Muller[a], Eugene Serabyn[a], Stuart B. Shaklan[a], John T. Trauger[a], Daniel W. Wilson[a], Scott D. Horner[b], Yalan Mao[b], Stephen F. Somerstein[b], Gopal Vasudevan[b], Douglas M. Kelly[c], Marcia J. Rieke[c]
[a]Jet Propulsion Laboratory, 4800 Oak Grove Drive, Pasasdena, CA, USA 91109; [b]Lockheed Martin Advanced Technology Center, Palo Alto, CA, USA 94303; [c]University of Arizona, Tucson, AZ, USA 85721

ABSTRACT

The NIRCam instrument on the James Webb Space Telescope will provide coronagraphic imaging from λ=1-5 μm of high contrast sources such as extrasolar planets and circumstellar disks. A Lyot coronagraph with a variety of circular and wedge-shaped occulting masks and matching Lyot pupil stops will be implemented. The occulters approximate grayscale transmission profiles using halftone binary patterns comprising wavelength-sized metal dots on anti-reflection coated sapphire substrates. The mask patterns are being created in the Micro Devices Laboratory at the Jet Propulsion Laboratory using electron beam lithography. Samples of these occulters have been successfully evaluated in a coronagraphic testbed. In a separate process, the complex apertures that form the Lyot stops will be deposited onto optical wedges. The NIRCam coronagraph flight components are expected to be completed this year.

Keywords: NIRCam, JWST, James Webb Space Telescope, coronagraph

1. INTRODUCTION

1.1 The planet/star contrast problem

Observations of extrasolar planet formation (e.g. protoplanetary disks) and planetary systems are hampered by the large contrast differences between these targets and their much brighter stars. For example, in reflected visible light Jupiter would appear only 10^{-9} as bright as the Sun to an observer in another star system, with an apparent maximum separation of only a few arcseconds as seen from the nearest star. Going further into the infrared wavelengths, where light from stars is decreasing, young (<1 GYr) massive planets glow on their own from thermal radiation. At about λ=4.5 μm the expected contrast between a young Jupiter and the star would be 10^{-3}-10^{-6}, making planet detection in this wavelength range much easier. Even at these more favorable contrasts, the instrumental glare caused by diffraction and scattering of starlight by a telescope's optics will overwhelm light from a planet and must be suppressed.

1.2 NIRCam coronagraph overview

The NIRCam[1] instrument on the James Webb Space Telescope (JWST) will provide imaging over λ = 1 – 5 μm and will have a coronagraphic mode for the suppression of diffracted starlight. It will be a premier tool in the coming decade for the detection of young, massive planets around nearby stars. The Lyot-type coronagraph comprises a variety of occulters located at the telescope focus and aperture masks (Lyot stops) located at subsequent images of the telescope pupil. Together these greatly suppress the prominent diffraction pattern of a star created by the hexagonally-segmented primary mirror and other obscurations in the telescope. Performance is expected to be limited by the scattered light created by uncorrectable optical wavefront errors that are budgeted for 131 nm RMS at the telescope focus[2].

Details of the NIRCam coronagraph and performance estimates have been previously provided[3,4]. Here we discuss the manufacture and testing of the coronagraphic occulters.

Techniques and Instrumentation for Detection of Exoplanets IV, edited by Stuart B. Shaklan, Proc. of SPIE
Vol. 7440, 74400W · © 2009 SPIE · CCC code: 0277-786X/09/$18 · doi: 10.1117/12.826448

2. OCCULTER DESIGN

2.1 Profiles and layout

NIRCam offers five apodized occulting patterns, three circular ones and two wedges. The circular patterns have a Bessel-squared ("sombrero") radial profile and the wedges have sinc-squared profiles perpendicular to the wedge long axes[3]:

$$T_{\mathrm{somb}}(r) = \left[1 - \left(\frac{2J_1(\sigma r)}{\sigma r}\right)^2\right]^2 \qquad T_{\mathrm{sinc}^2}(r) = \left[1 - \left(\frac{\sin(\sigma r)}{\sigma r}\right)^2\right]^2$$

T is the intensity transmission at radius r from the center of the pattern (perpendicular to the long axis for a wedge) and σ defines the size. The profiles are truncated past the first sidelobe. The graded transmissions offer better diffraction suppression than hard-edge occulters. The three circular occulters are scaled for 50% transmission at $r = 6\lambda/D$ radians (D is the telescope diameter, 6.55 m) at λ=2.1, 3.35, and 4.3 μm (0.40, 0.63, and 0.81 arcseconds, respectively). The wedges, each 20 arcseconds (12 mm) long, have 50% transmission at $4\lambda/D$ radians at the wedge centers at λ=2.1 and 4.6 μm (0.26 and 0.58 arcsec, respectively). They taper down to $2\lambda/D$ and expand to $6\lambda/D$. The five patterns exist on a single substrate. The occulter layout for one of the two NIRCam modules is shown in Figure 1. The layout is similar for the duplicate module with some of the patterns reordered. The field around each pattern is 20" x 20".

Along the top of the substrate are 5" x 5" neutral density (ND) squares of OD=3, and smaller 3" x 3" squares are arranged along the bottom. These will provide unsaturated acquisition images of the target star. The absolute pointing of JWST is not sufficient to accurately place the star behind the occulter, but the relative slews are more precise. So, the star will first be imaged within the large ND square nearest to the occulter. After its position has been measured with an automated centroiding algorithm it will be slewed to the smaller ND square located on the opposite side of the occulter (diagonal to the substrate long axis). The centroid will again be measured, providing both a more accurate location and an improved estimate of the roll orientation of the telescope. The star will then finally be slewed behind the occulter.

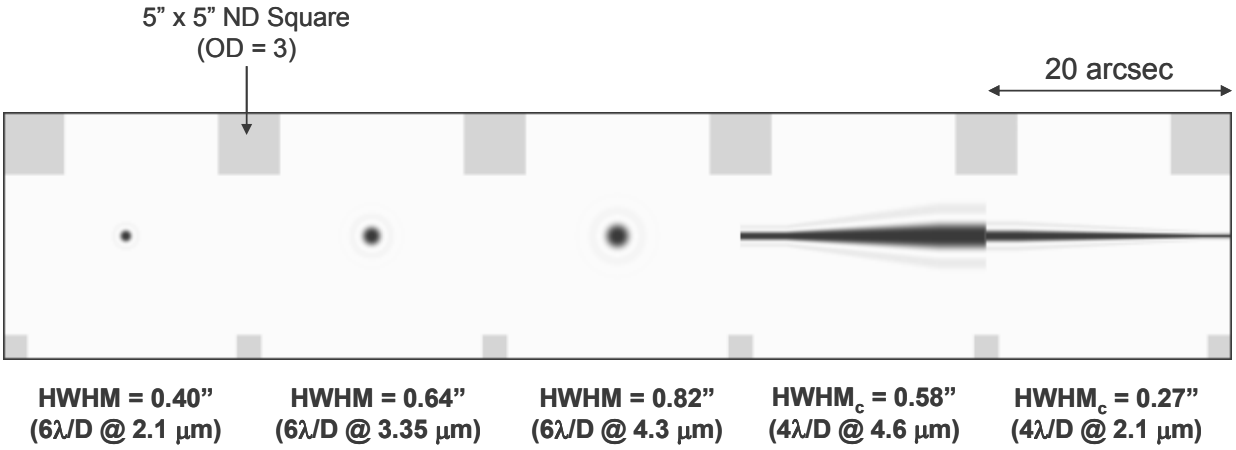

Fig. 1. Layout of the occulters and neutral density squares for one of the NIRCam modules (the layout of the occulters is different for the other NIRCam module). The area shown is 60 mm by 12 mm.

2.2 Defining the halftone pattern

Grayscale transmission occulters have been created using HEBS glass and metal deposition methods for visible wavelength coronagraphs[5-7]. However, these processes have not been extended to the λ = 1 – 5 μm range over which NIRCam operates. At present, only binary occulters appear to be viable for the NIRCam coronagraph. Halftoning provides a means to approximate a grayscale transmission profile with small dots[8].

The halftone pattern approximates the amplitude (square root of intensity) transmission of the specified occulter profile by altering the local density of the dots. In this case the dots cannot overlap and must be placed on a uniform grid (bitmap) with the same sampling as the dot size. Their distribution must be as random as possible to avoid periodic patterns that could create bright diffraction artifacts in the images. A single pattern is used for the circular occulters since it can simply be scaled in size to match the intended wavelength (with the dots scaled in size as well). Separate patterns must be defined for the short and long wavelength wedges, however.

2.3 Small hole effects and the choice of dot size

The occulters were initially defined using 0.8 μm diameter dots to create fine-grained approximations to the desired transmission profiles. This size was also the stated lower limit of the initial patterning vendor (which was unable to meet the specifications in the end). A series of occulters using this dot size were successfully produced at the Jet Propulsion Laboratory. Concerns were raised regarding possible anomalies that could be introduced by having holes that were smaller than the wavelength of incident light. Due to electromagnetic interactions with the material, the transmission of light through a subwavelength-diameter hole is nonlinear in relation to the hole's diameter, quickly decreasing as the hole becomes smaller than the wavelength[9]. Large phase shifts are also introduced, and together these effects could alter the effective occulter profile and perhaps introduce artifacts.

It is not obvious that the subwavelength effects would be significant for the NIRCam occulters. First, the fraction of subwavelength-sized holes decreases rapidly from the center as the dot density decreases with increasing transmission. The alteration of the pattern would be confined to a narrow region. Second, the estimated errors introduced are significantly less than the budgeted JWST wavefront aberrations. Were JWST a dedicated high contrast system with wavefront control, this would be a more important issue.

To allay concerns regarding potential subwavelength-hole effects, the dot sizes for the circular occulters were redefined to be equal to the central wavelength of the bandpass at which each occulter is intended to be used (2.1, 3.35, and 4.3 μm). The dots for the two wedges are 2.0 μm and 4.0 μm. Scaling the dot size with wavelength has an added benefit for testing as the coronagraphic testbed used (described later) operates up to only $\lambda = 2.5$ μm. The effectiveness of a halftone occulter can be evaluated using a pattern with wavelength-sized dots and from the results the effectiveness of the same pattern can be extrapolated to longer wavelengths.

The coarser granularity of the patterns having larger dots results in both a less accurate approximation of the desired profile, reducing diffraction suppression, and increased scattering. These effects were evaluated using diffraction models that included aberrations that matched the JWST wavefront error budget. The larger dots result in an increase in scattered light of about 3x compared to the 0.8 μm dots in an aberration-free system. However, the increased scatter is still nearly an order of magnitude lower than that caused by the JWST optical aberrations. Even if the JWST wavefront errors were only half of the budgeted levels (extremely unlikely), the coronagraphic performance would not be impacted by the larger dots.

Another potential issue with the larger dot size is the change in the scattering pattern caused by pointing errors of the star on the occulter. This is a factor because the coronagraphic observations by themselves will not provide sufficient contrast to achieve the science goals. The coronagraph will reduce the surface brightness of the star's point spread function by a factor of 4 – 10, past which contrast will be limited by the scattered light from the JWST optics. By relying on the optical stability of JWST, and hence the stability of the scattered light pattern, this residual starlight may be greatly reduced using PSF subtraction. The star can be observed at two roll orientations of the telescope, or an additional star can be imaged with the same configuration. In either case, one image can be subtracted from the other, removing the scattered light either down to the detector noise limit or to the residual level imposed by mismatches in the scattered light pattern between the two images. Each time the telescope is moved (rolled or slewed to new coordinates) the star will be repositioned on the occulter. If the alignments of the star on the occulter are different between the two images, the scattered light distribution will be different as well. The JWST pointing accuracy is expected to be between 10 – 20 milliarcseconds, which is 6 – 12 μm on the occulter. This is a few dots worth of offset when using a λ=2.1 μm occulter (the PSF at this wavelength will have a full-width-at-half-maximum of about 40 microns at the occulter). Diffraction models show that the residual levels set by such offsets would be the same for a grayscale occulter and a halftone one using 0.8 μm dots. At λ=2.1 μm the residual level will be about 2x greater using the 2.1 μm dots while at λ=4.3 μm with 4.3 μm dots the levels will be about the same as with the smaller dots or grayscale. Thus, there is no significant disadvantage to using the wavelength-sized dots in regards to residuals caused by pointing errors.

2.4 Pattern tolerancing

There are no high contrast imaging requirements on JWST, and the NIRCam coronagraph is not considered an official critical JWST component. The coronagraphic performance is dominated by the uncorrected JWST wavefront errors, so small errors in the occulters will not result in large degradations in contrast. Therefore, the coronagraph tolerances are not rigidly defined and are subject to modification by the NIRCam Science Team as manufacturing and cost constraints change. However, some general performance goals have been established to meet particular science interests[3,4]

The measured mean transmission profile of an occulter should not deviate by more than 5% from the specification in the radial direction. This defines an envelope for an acceptable profile by scaling the desired profile by ±5% in size. This ensures that the occulter provides the required inner working angle and the correct profile for diffraction suppression (the Lyot stops are designed to work with occulters having the specified profile). The maximum optical density of an occulter must also be OD>4 to prevent leakage of starlight (this sets the minimum thickness of the aluminum layer that forms the dots).

In addition to the tolerances on any deviations in the profile, there are also limits on any dust particles or residual spots of Al/Cr coating that may not be properly etched away. Modeling experiments suggest that one or two random stray spots of 30 – 50 μm will not compromise diffraction suppression performance, especially if the spots are more than a few λ/D radians away from the occulter center. The greater concern is that any stray spots near the occulter could block a planet, so limits have been established on their sizes and distances relative to the occulter centers.

3. OCCULTER FABRICATION

3.1 Substrate and mounting

Each flight occulter substrate is a 66 mm by 22 mm by 2 mm sapphire slide of which the mounting fixture exposes a 60 mm by 12 mm area. Each substrate is permanently mounted near the entrance of a NIRCam module at the focus of the telescope, just outside the normal NIRCam field of view. Each module has a different field of view, so only one will be used for coronagraphic imaging for a given observation. No on-orbit adjustments can be made to the occulter position. A star is placed onto the occulter by offsetting the telescope; this redirects the beam from its normal path within the camera and it would end up outside of the detector, so an optical wedge located at the Lyot stop restores its direction. Integrated into the backside of the mounting are two light emitting diodes that will be used as artificial point sources to occasionally monitor the NIRCam internal alignment and wavefront errors.

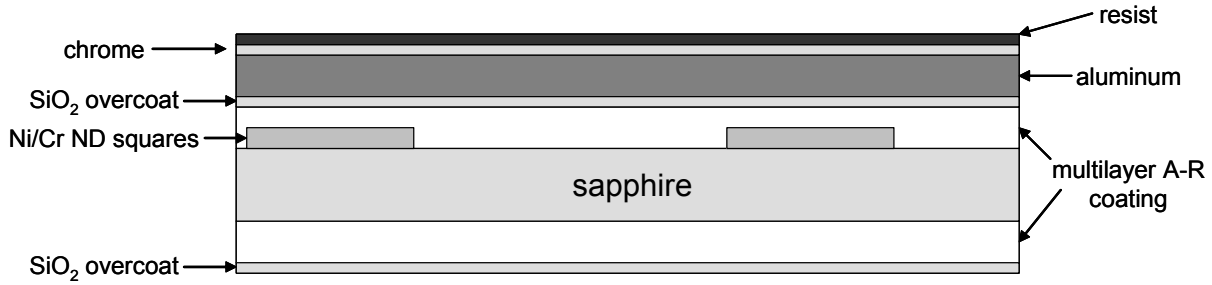

Fig. 2. Schematic diagram, not to scale, of the coatings on a NIRCam occulter substrate prior to lithographic patterning. Barr Associates deposits the ND squares, A-R coating, and SiO_2 overcoat. JPL/MDL applies the resist and then creates the dots by exposing the resist to an electron beam and then etching away the Al and Cr in the unexposed areas.

3.2 Coatings and pattern etching

The coating of the flight substrates (Figure 2) is being done by Barr Associates under contract to the NIRCam project at the University of Arizona. The nickel-chrome ND squares are first deposited onto the bare substrate, and then multilayer SiO_2 antireflection coatings are applied on both sides. The coating is designed to provide high transmission and low mean reflectivity between $\lambda = 2 – 5$ μm (optimized more towards the longer wavelengths), with enough transmission at $\lambda = 0.633$ μm to allow for optical alignment using a HeNe laser. A 180 nm-thick layer of aluminum is then deposited on

the front surface (the side with the ND squares) followed by a 20 nm-thick layer of chrome. The coated substrates are then sent to the Micro Devices Laboratory (MDL) at the Jet Propulsion Laboratory (JPL), where a layer of resist is deposited on the front surface.

In the lithographic patterning process, the dots comprising the halftone occulters are created by exposing areas of the coated substrate to an electron beam (e-beam), which hardens the resist. The patterns were provided to MDL as bitmapped images. The aluminum and chrome top layers under the unexposed resist are then removed using wet and plasma etching. The chrome protects the aluminum lay to reduce undercutting during etching, which would produce undersized dots.

Before attempting fabrication of the patterns on the candidate flight substrates, a series of "pathfinder" test samples were produced (Figure 3). These utilized a variety of round and rectangular SiO_2-overcoated sapphire and bare fused silica substrates. The coating and patterning of these test samples were done at MDL. The initial ones were created with halftone patterns of 0.8 μm square dots, and later ones had the wavelength-sized square dots used on the flight occulters. Some of the samples included multiple copies of the same patterns created with different levels of e-beam exposure to determine the optimal doses (which defines the size of the dots). The SiO_2-overcoated sapphire samples were also used to determine how much of the antireflection coating will be removed by the etching process.

Two flight-quality substrates coated by Barr will be patterned by MDL and evaluated using the testing procedures described in Section 4. Two flight-qualified, patterned substrates for each module will be delivered by JPL as well as one spare for one of the modules. As these masks must remain pristine, they will not be subjected to testing except for verification of the pattern under a microscope in a clean room. A yield of 50% is assumed, so at least 10 flight candidates will be coated.

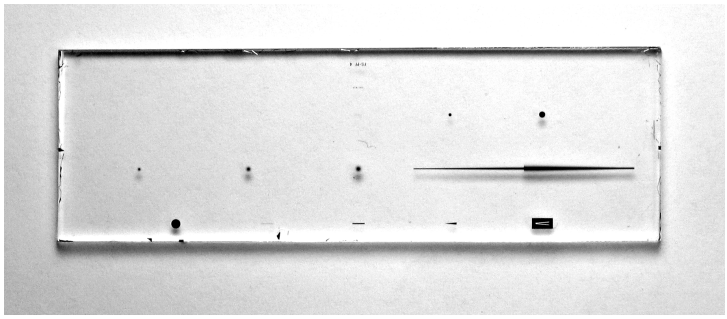

Fig. 3. An example of a pathfinder test sample. This is an uncoated 66 mm by 21 mm fused silica substrate with the five NIRCam occulter patterns. Additional patterns for microscope calibration were included above and below the occulters. Small regions of residual coating exist because the fabrication process for this test piece did not use flight-level standards.

4. OCCULTER TESTING

4.1 Pattern verification

All of the pathfinder patterns were scanned with a digital camera on an optical transmitted-light microscope (Figures 4 and 5). In addition, small regions of some patterns were measured using an atomic force microscope (Figure 6). Electron microscopy (EM) was used only on one SiO_2 substrate sample and could not be used on the sapphire samples as the electrical contrast between aluminum dots and the sapphire substrate (aluminum oxide) was too small to provide an image.

The profiles of the occulters were derived from the microscope images and compared to the specifications (Figure 7). To do so, an image was first divided by a flat field (an image of a clear region of the substrate taken at the same exposure level) to account for uneven illumination. The zero level was computed using the mean value within the center of the occulter where there are no holes and subtracted. The image was then renormalized to have a transmission of 1.0 in the clear regions. The mean profiles for the circular occulters were derived by computing the mean value of all image pixels located on a circle centered on the occulter at each radius (i.e. the fraction of clear transmission compared to the circumference of the circle at that radius). For the wedges, where the long wedge axes are oriented horizontally in the images, the mean values in each row over 21 columns were computed at different locations along the wedges.

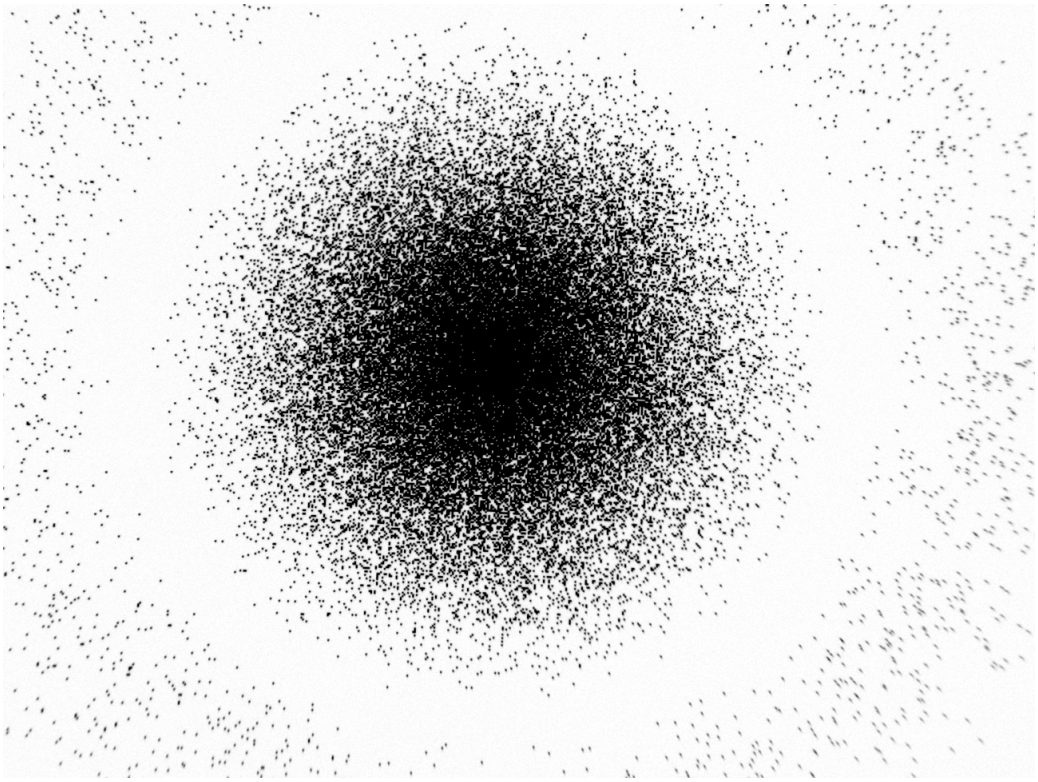

Fig. 4. Optical transmission microscope image (10x objective) of the circular occulter pattern on a pathfinder test sample scaled for λ=1.65 μm (1.65 μm dots). The outer ring of the occulter is truncated by the camera's field of view (1.29 mm by 0.97 mm at this magnification).

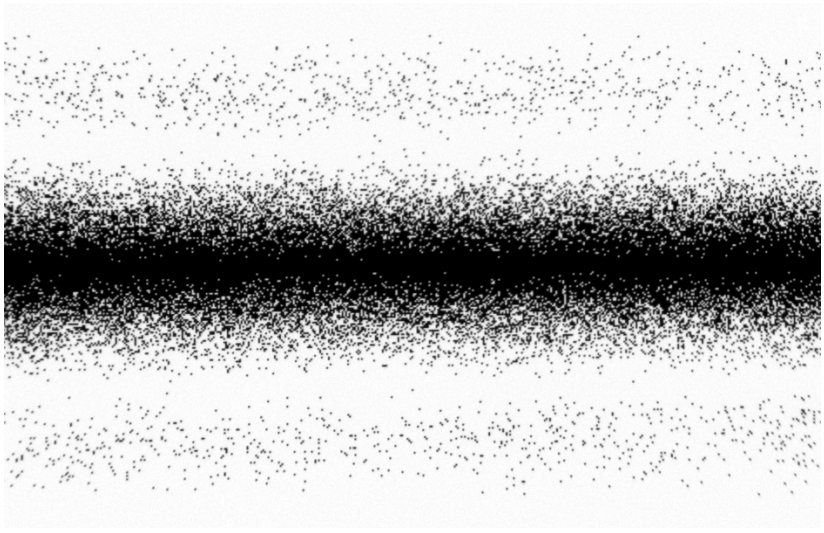

Fig. 5. Optical transmission microscope image (10x objective) of the narrow end of the short wavelength wedge (2.0 μm dots).

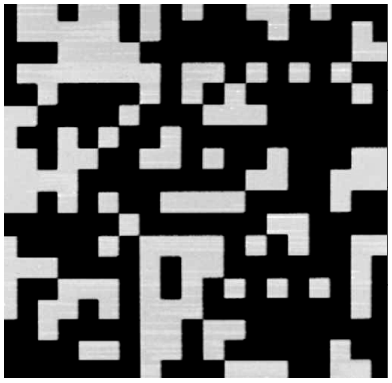

Fig. 6. Atomic force microscope measurement of a section of the small circular NIRCam occulter (2.1 μm dots) on a pathfinder test sample. The bright areas are the dots, the dark are clear regions.

4.2 Testbed verification

While computer models predicted that the halftone occulters would work without introducing significant artifacts, it was considered prudent to actually test some of the patterns in a real optical system, the Infrared Coronagraph Testbed (IRCT) at JPL. The IRCT is used to test the performance of new coronagraphic systems, some prior to installation at the 5 meter Hale telescope at Palomar Observatory. The input point source is a fiber fed by either a laser or Fianium supercontinuum light. Off-axis reflective optics are used except for a lens that reimages the pupil after the occulter. The system in the configuration used for the tests produced an f/18 beam, identical to the JWST focal ratio. The system has a circular, unobscured pupil that is focused onto the occulter, followed by reimaging optics that create an image of the entrance pupil (this reimaged pupil is where the Lyot stop is located). An infrared digital camera capable of imaging up to $\lambda = 5$ μm was used, though the supercontinuum source is only useful out to $\lambda = 2.5$ μm.

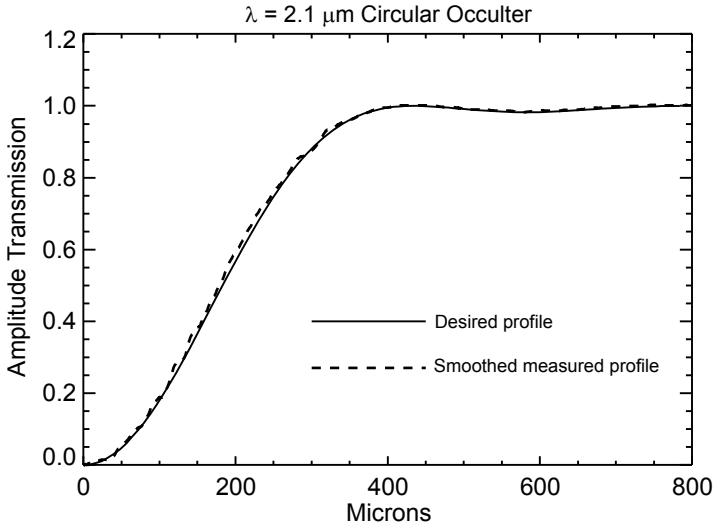

Fig. 7. Measured (smoothed) and desired amplitude transmission profiles of the small NIRCam circular occulter (for λ=2.1 μm with 2.1 μm dots). The measured profile was derived from a microscope image.

Images were taken at $\lambda = 1.65$ and 2.2 μm with H and K bandpass filters, respectively. These used the circular occulters with 1.65 μm and 2.2 μm dots (custom made for testing). Images were taken at the reimaged pupil prior to the Lyot stop and at the final image plane. The pupil image is especially useful for indirectly verifying the profile of the occulter. With a circular, unobscured entrance pupil, a circular occulter at the intermediate focus will result in reimaged pupil that looks like a ring. The cross-section of the ring is sensitive to the occulter profile – if the central core of the occulter is too sharp-edged there will be additional ringing around the primary ring, for instance. Ideally, there will be just a single ring with a dark line running through the middle.

The images of the reimaged pupil are shown in Figure 8 and 9. Figure 8 shows the pupil created by an occulter produced by a non-MDL vendor that had the wrong dot size and thus an incorrect profile. The effect of the error is clearly demonstrated by the ringing in the pupil. The pupil shown in Figure 9 produced by a correct occulter exhibits the single ring bisected by a dark line as expected. The pupil interiors are not completely dark due to aberrations and dust in the testbed (the features are there regardless of which occulter is used). Figure 10 shows the image at the final focus of the system demonstrating the diffraction pattern suppression of the coronagraph down to the level of the testbed aberrations.

Fig. 8. Image from the IRCT of the reimaged pupil following the occulted point source. The circular occulter used was sized for λ=2.1 μm and the image was taken at λ=1.55 μm. This initial sample, which was created by a non-MDL vendor, used a pattern designed for 0.8 μm diameter dots but manufacturing errors resulted in 2.4 μm ones. The larger dots resulted in a more opaque transmission profile with a flatter center. This resulted in creating multiple rings in the reimaged pupil that provided evidence that the pattern was incorrect. Some ghosts from the testbed setup are visible.

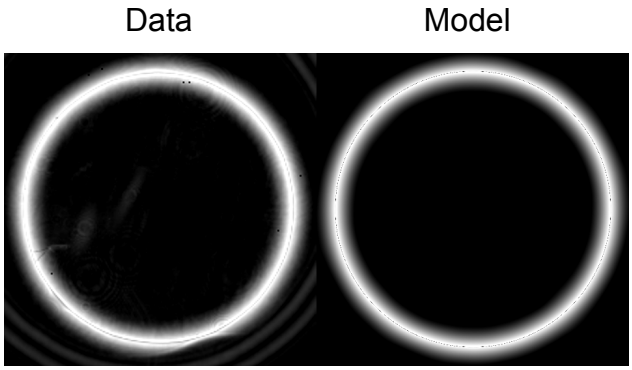

Fig. 9. Actual IRCT halftone occulter (left) and theoretical greyscale occulter (right) images of the reimaged pupil after occultation of a point source in H band (λ=1.65). The NIRCam circular occulter halftone pattern was used scaled to λ=1.65 μm with 1.65 μm dots. The agreement between both images show that the occulter was performing as expected. The real data shows testbed aberrations inside of the pupil, a double ring of a ghost image outside of the pupil, and a clipping along the lower edge due to an intervening aperture.

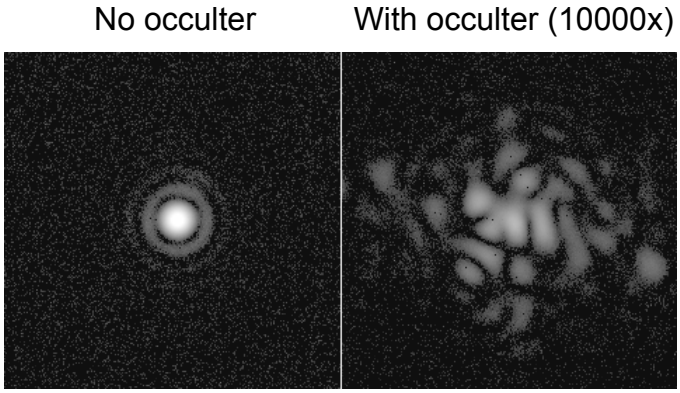

Fig. 10. Focal plane images from the IRCT in K band (λ = 2.2 μm), displayed as the quarter-root of intensity. (Left) Image with a circular Lyot stop in place but no occulter. (Right) Image with the 2.2 μm dot pattern mask and Lyot stop in place, multiplied by 10000 in intensity to compare with the image on the left. The speckles are due to aberrations in the testbed.

4.3 Environmental testing

Some additional tests were conducted on the pathfinder samples to evaluate their resiliency (these will also be done to the flight-quality engineering samples). The adhesion of the dots was tested by applying a piece of tape to a substrate and then pulling it off as recommended by MIL Std C-48497A. Examinations of both the substrate and the tape under a microscope showed that no dots were removed. Another sample was gently rubbed with an alcohol-soaked cotton swap to test abrasion resistance during cleaning (recall that the dots do not have a protective overcoating). Under the microscope some debris was seen, perhaps dislodged chrome layers. Therefore, it was recommended that abrasive cleaning not be used (alcohol rinsing is acceptable). Since, JWST will be passively cooled to cryogenic temperatures, a piece of another patterned sapphire sample was submerged three times into a dewar filled with liquid helium, exposing it to temperatures as low as 10 K. Each cycle was much more rapid than would occur on JWST. The patterns and substrate appeared unaffected.

5. LYOT STOPS

As of the time of writing, the Lyot stops have yet to be manufactured. They will be metallic coatings deposited onto optical wedges that will be located in the pupil/filter wheel inside each channel of each NIRCam module. The wedges divert the off-nominal coronagraphic beam paths back onto the detectors.

There are two Lyot stops in each wavelength channel, one for the wedge occulter and another for the circular occulters (Figure 11). The wedge occulter stop consists of polygonal holes that are defined by vertex coordinates. The circular occulter stop has rounded holes defined by many points. Due to distortion of the pupil inside NIRCam, these coordinates must be projected using ray tracing software onto the wedges. Because of chromatic distortion and aberrations introduced by the refractive pupil imaging assembly, the short wavelength Lyot stop may not be effective below $\lambda = 2$ μm.

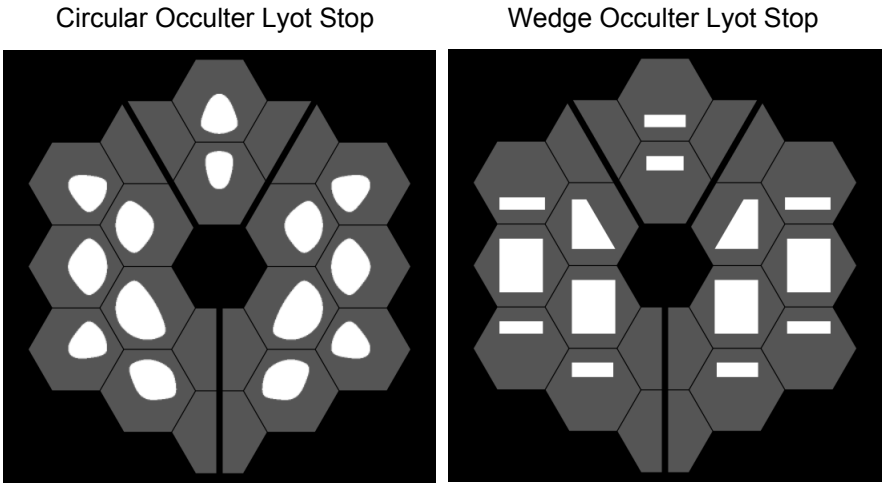

Fig. 11. Schematic representations of the NIRCam Lyot stops for (left) the circular and (right) wedge occulters. The clear regions of the stops are shown in white projected onto the JWST entrance pupil (grey). In reality, the stops will be warped to match the distortion of the pupils within NIRCam.

6. CONCLUSIONS

The components of the NIRCam coronagraph are currently under construction. Prototype halftone occulters have been successfully fabricated and demonstrated in a coronagraphic testbed. These are especially important as there are no pre-launch performance tests of NIRCam planned in its coronagraphic mode. The coating and patterning of the flight substrates is underway, and they will be delivered by the end of 2009. The Lyot stops are expected to be generated later

this year or early next year. The measured prototype performance and simulations of the flight system indicate that the NIRCam coronagraph should be a great advance in the imaging of extrasolar planets in the next decade.

ACKNOWLEDGEMENTS

The research described in this publication was carried out at the Jet Propulsion Laboratory, California Institute of Technology, under a contract with the National Aeronautics and Space Administration.

REFERENCES

[1] Horner, S., Rieke, M., NIRCam team, "The Near Infrared Camera (NIRCam) for the James Webb Space Telescope (JWST)", Proc. SPIE, 5487, 628 (2004).

[2] Lightsey, P. A., Barto, A. A., Contreras, J., "Optical performance for the James Webb Space Telescope", Proc. SPIE, 5487, 825 (2004).

[3] Krist, J. E., Beichman, C. A., Trauger, J. T., Rieke, M., J., Somerstein, S., Green, J. J., Horner, S. D., Stansberry, J. A., Shi, F., Meyer, M. R., Stapelfeldt, K. R., Roellig, T. L., "Hunting planets and observing disks with the JWST NIRCam coronagraph", Proc. SPIE, 6693, 66390H (2007).

[4] Green, J. J., Beichman, C., Basinger, S. A., Horner, S., Meyer, M., Redding, D. C., Rieke, M., Trauger, J. T., "High contrast imaging with the JWST NIRCam coronagraph", Proc. SPIE, 5905, 59050L (2005).

[5] Moody, D. C., Gordon, B. L., Trauger, J. T. "Design and demonstration of hybrid Lyot coronagraph masks for improved spectral bandwidth and throughput", Proc. SPIE, 7010, 70103P (2008).

[6] Balasubramanian, K., "Band-limited image plane masks for the Terrestrial Planet Finder coronagraph: materials and designs for broadband performance", Applied Optics, 47, 116, (2008).

[7] Balasubramanian, K., Wilson, D. W., Muller, R. E., Kern, B. D., Sidick, E., "Thickness-dependent optical properties of metals and alloys applicable to TPF coronagraph image masks", Proc. SPIE, 6693, 66930Z (2007).

[8] Vasudevan, G., Reale, M., Somerstein, S. F., "Some performance results from NIRCam's coronagraphic prototype masks", Proc. SPIE, 5904, 590408 (2005).

[9] Genet, C., Ebbesen, W., "Light in tiny holes", Nature, 445, 39 (2007).